1 **Title**

2 Altered drug metabolism and increased susceptibility to fatty liver
3 disease in myotonic dystrophy

4

5 **Author list**

6 Zac Dewald[1], Andrew Gupta[1], Ullas V. Chembazhi[1], and Auinash Kalsotra[1,2,3§]

7 **Affiliations**

8 [1]Department of Biochemistry, [2]Cancer Center@Illinois, and [3]Carl R. Woese Institute for
9 Genomic Biology, University of Illinois, Urbana-Champaign, IL, United States.

10 [§]To whom correspondence should be addressed: Auinash Kalsotra, Ph.D.

11 506 South Mathews Ave, Medical Sciences Building, Room 462, Urbana, IL 61801

12 Phone: 1-217-300-7654; Fax: 1-217-244-5858; E-mail: kalsotra@illinois.edu

Abstract

Myotonic Dystrophy type 1 (DM1), a prevalent muscular dystrophy affecting 1 in 2800 individuals, is associated with a toxic $(CTG)_n$ repeat expansion in the *DMPK* gene. While DM1 affects multiple systems, recent studies highlight its link to liver pathology, glucose intolerance, and drug sensitivity. Our study focused on liver implications by creating a hepatocyte-specific DM1 mouse model. Expression of toxic RNA in hepatocytes sequestered muscleblind-like (MBNL) proteins, impacting hepatocellular activity. DM1-induced liver alterations included morphological changes, inflammation, necrosis, and fatty accumulation. Impaired drug metabolism and clearance were evident in DM1 mice and increased susceptibility to diet-induced fatty liver disease. Notably, alternative splicing of acetyl-CoA carboxylase 1 induced excessive lipid accumulation in DM1 livers, exacerbated by high-fat, high-sugar diets. These findings unveil disruptions in hepatic functions, predisposing DM1 livers to injury, fatty liver disease, and compromised drug clearance. Understanding these mechanisms is crucial for addressing the complex health challenges in DM1 patients and optimizing treatment strategies.

Introduction

Myotonic Dystrophy Type 1 (DM1) is an autosomal dominant disease and the second most common form of muscular dystrophy, affecting more than one in three thousand adults in North America[1–3]. The cardinal symptoms of DM1 include myotonia, debilitating muscle weakness and wasting, abnormal heart function, and excessive fatigue[1,2]. Despite DM1's initial characterization as a form of muscular dystrophy, the disease is genuinely multisystemic; patients report various gastrointestinal, metabolic, and neurological dysfunctions, such as excessive daytime sleepiness and insulin resistance[2,4].

DM1 is caused by a (CTG)n repeat expansion in the 3' UTR of a ubiquitously expressed gene Dystrophia Myotonica protein kinase (*DMPK*)[5–7]. The (CUG)n containing RNAs resulting from the transcription of the diseased *DMPK* gene form hairpin secondary structures and aggregate in the nucleus, forming discrete RNA foci[7,8]. These foci interact with and sequester the muscle blind-like (MBNL) family of splicing factors[9,10]. MBNL proteins affect many developmentally-regulated alternative splicing and polyadenylation decisions in various tissues throughout the process of maturation towards adulthood; thus, their loss-of-activity in DM1 shifts splicing of target pre-mRNAs towards preadolescent-like patterns, inducing specific features of the disease[11–14]. This reversal of transcriptomic patterns from mature-to-immature state drives many disease symptoms to become more prevalent later in life, with diagnosis often occurring in the mid to late thirties[12,15,16]. However, diagnosis typically occurs only after the development of significant muscular or neurological symptoms, which allows for the subtle and long-term consequences of the disease to go unmanaged[16].

DM1 patients are abnormally sensitive to a wide range of anesthetics and muscle relaxants, resulting in prolonged anesthesia recovery, heightened pulmonary dysfunction,

and, in some cases, death[1,17,18]. The disruption of neurological and muscular function, hallmarks of DM1, is often blamed for this sensitivity. However, within the last twenty years, several studies have demonstrated that DM1 patients have an increased susceptibility to non-alcoholic fatty liver disease (NAFLD), metabolic syndrome, and liver damage[19–22]. These studies would suggest inappropriate liver function and a predisposition for liver injury in DM1 patients. A malfunctioning liver could also help explain the sensitivity to anesthetic treatment; a liver that cannot provide adequate metabolism of xenobiotic material would prolong the clearance time for many drugs and may increase their potency. Minor malfunctions in liver response to metabolic signaling and drug metabolism may frequently occur in DM1 patients; however, none have investigated this possibility.

Here, we sought to determine what effects DM1 might have on hepatic functions and overall liver health. Utilizing two previously established mouse lines, we generated a mouse model in which we induced the expression of (CUG)960 repeat-containing RNA, specifically in the hepatocytes within the liver[23–25]. Combining acute and long-term DM1 liver mice models with systematic biochemical, molecular, and high-resolution transcriptome analyses, we found that toxic (CUG)960 RNA expression triggered global gene expression and RNA processing defects in the hepatocytes. These transcriptome defects led to various physiological and cellular pathologies, including accumulation of lipids and fatty liver, increased susceptibility to insult and injury, and misregulation of xenobiotic metabolism. Specifically, we uncovered that aberrant splicing and upregulation of Acetyl CoA Carboxylase 1 (ACC1), the rate-limiting enzyme for *de novo* fatty acid biosynthesis, drives the NAFLD phenotype in DM1-afflicted mice livers. Importantly, both the fatty liver and the poor drug metabolism phenotypes are intrinsic to the repeat RNA toxicity within hepatocytes, as these

defects were not detected in transgenic mice, which express the repeat RNA only in the muscle tissues. Thus, our study reveals that DM1 disrupts normal hepatic functions, predisposes the liver to fatty liver disease and injury, and confirms the need for further research into the effects of DM1 in non-traditional tissues, including the liver.

Results

A hepatocyte-specific murine model of DM1 recapitulates the molecular features of the disease in the liver

The pathogenic mechanism of DM1 is comprised of three primary parts: i) the transcription and production of a long CUG repeat-containing RNA, ii) the accumulation of this RNA into nuclear foci, and iii) the sequestration of MBNL proteins into such RNA foci, which results in the decrease of MBNL directed RNA processing activities[26–28]. To study the effects of DM1 within the liver, we generated a bi-transgenic murine model by combining two existing mice models. First is the tetracycline-inducible mouse model with a *DMPK* transgene containing the last five exons of human *DMPK* and 960 interrupted CTG repeats (labeled here as CUG960i RNA), developed by Cooper and colleagues[23]. The second model utilizes the expression of a reverse tetracycline trans-activator (rtTA) driven by a liver-specific apolipoprotein E (ApoE) promoter, which is highly expressed in hepatocytes[24]. By crossing these two mice models, we generated a double homozygous bi-transgenic line that allows for conditional, doxycycline (Dox)-dependent expression of the CUG960i RNA specifically in the liver tissue, thus allowing the study of DM1 disease in the liver (Fig. 1a). From now on this bi-transgenic model is referred to as the DM1 liver model. The control mice for this model contain only the homozygous ApoE-rtTA allele.

To mimic the DM1 conditions seen in human patients, we induced the disease in newborn pups by feeding the mother a diet supplemented with 2 g of Dox per kg of chow. Once weaned, mice then continued a Dox diet at a lower dose of 0.1 g/kg until they reached adulthood at nine weeks (Fig. 1b). At eight weeks of age, mice were fasted for 20-22 hours and administered a glucose tolerance test (GTT).

To confirm the appropriate expression of the CUG960i RNA and the formation of toxic RNA/RNA binding protein (Rbp) foci, we utilized fluorescent in-situ hybridization and immunofluorescence (FISH-IF) imaging with probes targeting the CUG repeat sequence within the RNA (Fig. 1c). Bright puncta of condensed CUG RNA were seen in the nuclei of most hepatocytes. The signal from these RNA foci overlapped with the immunofluorescent signal when fluorescent MBNL1 or MBNL2 antibodies were used, indicating that the toxic CUG RNAs have successfully sequestered the MBNL proteins. The MBNL-containing RNA foci only occurred in the DM1 mice's livers and not in the ApoE-rtTA control mice's livers.

Quantification of the CUG960i/MBNL foci indicated that over 80% of hepatocyte nuclei in the DM1 mice contain at least one RNA focus, ensuring the uniformly distributed expression of both transgenes (Fig. 1d). The appearance of RNA foci was Dox-dependent — when mice with both the ApoE-rtTA and CUG960i alleles were not fed Dox or if the Dox diet was withdrawn for a week or more, the RNA foci were undetectable. The distribution of CUG960i RNA foci per nuclei followed a Poison curve, with most hepatocytes having one to three foci and a small number of hepatocytes exceeding ten plus foci within a single nucleus (Fig. 1e).

Finally, to assay the amount of toxic RNA produced, CUG960i transgene expression was quantified by isolating RNA from whole livers and conducting qPCR using primers located in the final exon of the *Dmpk* transcript. DM1 liver mice expressed the CUG960i transgene at levels near ten percent of *β-actin* transcripts within the liver, compared to ApoE-rtTA control mice, which showed no evidence of CUG960i expression (Fig. 1f). A comparison of CUG960i RNA within isolated hepatocytes versus that of the

whole liver confirmed that the transgene's expression occurs primarily within hepatocytes (Supplementary Fig. 1a, b). Livers of the bi-transgenic mice not fed Dox showed no CUG960i expression, confirming that Dox must be provided to these animals to express sufficient amounts of toxic RNA. (Fig. 1f).

Expression of CUG960i RNA induces global transcriptomic changes within hepatocytes

Upon establishing that the DM1 liver model reproduces the molecular features of the disease, we prepared total RNA from purified hepatocytes isolated from the ApoE-rtTA controls and DM1-afflicted mice fed a 2.0 g/kg Dox-supplemented diet for nine weeks. We next assessed the splicing patterns of MBNL1-regulated exons within these RNA samples using end-point reverse-transcription PCR (RT-PCR) assays. The DM1 mouse livers consistently reproduced an alternative splicing pattern that significantly deviated from the control samples (Fig. 2a), confirming that, like the muscle and brain tissues, the expanded CUG repeat-containing RNA of DM1 also induces splicing defects in the liver.

We next performed high-resolution RNA sequencing of poly(A) selected RNA from the purified hepatocyte samples to further explore the genome-wide RNA processing defects in DM1-afflicted livers. Analysis of the resulting data revealed widespread changes in the DM1 hepatocyte transcriptome, with significant changes in mRNA abundance, splicing, and alternative polyadenylation (ApA) (Fig. 2b). Focusing on gene expression, inducing DM1 within the murine liver changed the mRNA abundance of 760

148 transcripts at a 2-fold level or higher, with 516 upregulated and 244 downregulated
149 compared to control livers (Fig. 2c).

150 As the MBNL proteins are most known for regulating alternative splicing events, it
151 is not surprising that nearly one thousand splicing events changed upon the expression
152 of the CUG960i RNA within the liver. Of the 928 splicing events that demonstrated a
153 greater than 10% change in PSI (Percent Spliced In) within the DM1 liver, every type of
154 alternative splicing event was represented, with most falling under the category of
155 cassette exons, and 35 of those events showing a ΔPSI change of 50% or higher (Fig.
156 2d, Supplementary Fig. 1c). Using RT-PCR, forty-one of these alternatively spliced events
157 were validated; the comparison showed a high consistency between the RNA-seq and
158 RT-PCR results (Fig. 2, e).

159 Gene ontology analysis of the transcripts experiencing dysregulation in
160 abundance, splicing, or ApA revealed enrichments in unique functional categories.
161 Transcripts changing in abundance were enriched in glucose, lipid, and energy-related
162 metabolism, as well as oxo-reductase and cytochrome p450 activities (Fig. 2i,
163 Supplementary Table 1)[29]. The transcripts with altered splicing patterns were enriched in
164 mRNA processing, signal transduction, and protein phosphorylation. A substantial
165 number of transcripts encoding proteins associated with the immune response,
166 specifically the response to viral and bacterial infection, exhibited defects in both overall
167 abundance and splicing (Fig. 2j, Supplementary Tables 1-3). Transcripts with
168 misregulated ApA events, much like misregulated splicing events, were enriched in
169 nucleotide binding, protein binding, and transport-related functions.

The proposed molecular mechanism of DM1 entails disrupting MBNL protein activities, resulting in a transcriptomic shift away from the normal state of healthy adult tissue and towards an immature state in the muscles, heart, and neurons[13,27,28,30,31]. To test whether this pattern holds within the liver, we isolated hepatocytes from *Mbnl1*$^{\Delta E3/\Delta E3}$ (*Mbnl1* knockout) mice and corresponding littermate wild-type controls at ten weeks of age[32]. Again, RT-PCR splice assays were performed on the poly(A) selected RNAs purified from wildtype and *Mbnl1* KO hepatocyte samples, and the results were compared to the DM1 liver and ApoE control samples. Notably, the DM1 liver samples showed a shift in splicing away from controls in the same direction as the *Mbnl1* KO samples (Fig. 2f; Supplementary Fig. 1d, e). However, the DM1 samples often demonstrated a more significant deviation from “normal” than the *Mbnl1* KO samples.

This prompted a full comparison of differentially expressed genes and alternatively spliced events between the DM1 and *Mbnl1* KO hepatocyte transcriptomes via RNA-Seq. Of the 705 alternatively spliced events in DM1 hepatocytes and the 508 that occurred in the hepatocytes of *Mbnl1* KO mice (difference in ΔPSI > 15%), only 175 events were common to both sets (Supplementary Fig. 1f). A similar pattern was observed for differentially expressed genes, with only a 15% overlap between the DM1 and *Mbnl1* KO data sets (Supplementary Fig. 1g). This limited overlap was surprising, as MBNL1 sequestration is a crucial driver of the transcriptomic defects in DM1 heart and muscle tissues.

As MBNL proteins promote tissue maturation and function, we next compared the transcriptomic changes in hepatocytes isolated from adult livers of DM1, *Mbnl1* KOs, and

wild-type mice livers during postnatal maturation[33]. By comparing alternatively spliced transcripts that change in either the context of DM1, *Mbnl1* KO, or liver maturation, we found that only about 25% of the events changing in DM1 were regulated by MBNL1 (Fig. 2g, h). Of note, whereas only a modest portion of mis-spliced events in DM1 were developmentally regulated, over 50% of transcripts changing in abundance in the DM1 liver were also developmentally regulated.

To explore the limited overlap between the hepatic transcriptomes of DM1 and *Mbnl1* KO mice with developing livers, potential compensatory mechanisms for MBNL1 function were investigated. We found that while MBNL1 levels are wholly depleted within the *Mbnl1* KO livers, MBNL2 levels were elevated 4-fold, as confirmed by western blot analysis (Supplementary Fig. 1h). The upregulation of MBNL2 might explain why there is lower-than-expected overlap between changes in the *Mbnl1* KO and DM1 liver models. Additionally, the increase of MBNL2 implies a compensatory mechanism that buffers the effects of Mbnl1 loss within the liver, a mechanism demonstrated in other tissues[34,35].

Hepatocyte-specific expression of CUG960i RNA induces increased lipid accumulation and liver injury

As the effects of DM1 in the liver are unstudied, and even the role of MBNL proteins in the liver is unknown, we took a generalized approach to assess the pathological consequences of DM1 within the liver. This process started before sacrifice, as blood glucose levels just before sacrifice indicate a slight difference in the blood glucose levels between male DM1 liver mice and male controls (Fig. 3a). However, this difference does not occur within the female groups (Supplementary Fig. 2a). There was also no difference

between DM1 liver mice and controls during glucose tolerance testing performed in the weeks before sacrifice (Fig. 3b; Supplementary Fig. 2b). Median mouse weight between female control and DM1 mice also showed no significant difference; however, DM1 male mice were 10-17% larger than ApoE-rtTA control males (Supplementary Fig. 2c). This increase in size is likely not due to the induction of DM1 in the DM1 liver mice, as male mice of this strain were larger than the ApoE-rtTA control males regardless of whether they were consuming a Dox diet.

As glucose intolerance is a common symptom in DM1, we compared GTT analysis from the DM1 liver mice and control mice against the HSA L/R mice, a DM1 model commonly studied for skeletal muscle pathologies[8]. The HSA L/R model expresses the toxic CUG repeat-containing RNA only within the muscle tissues, allowing us to compare the direct contributions of liver and muscle tissue toward glucose intolerance in DM1. While the HSA L/R mice showed significant glucose intolerance, the DM1 liver mice showed normal glucose handling (Fig. 3b).

Histological analysis of the DM1 mice livers using Hematoxylin and Eosin (H&E) staining revealed varying degrees of morphological changes and regions with decreased sinusoidal spacing within the DM1 livers (Fig. 3c). Additionally, increased lobular inflammation and necrotic patches were found within the DM1 livers (Fig. 3c).

DM1 patients have shown an increased susceptibility to fatty liver disease[19,20]. Therefore, we used Oil Red O staining on frozen mice liver tissues to interrogate the lipid accumulation within the DM1 liver model. Relative to the control animals, DM1 liver mice showed a significant increase in lipid droplets (Fig. 3c, d). While a long-term Dox diet can result in a modest accumulation of lipids in the liver, the DM1 mice consistently displayed

238 higher lipid levels, nearly twice that of respective controls. Furthermore, the mouse liver-
239 to-carcass weight ratio showed a significantly higher hepatosomatic index in DM1 liver
240 mice than in controls (Fig. 3e), with a median increase of 36.6%.
241
242 **DM1 liver model mice demonstrate decreased drug metabolism**
243 An often-reported challenge when treating DM1 patients is their increased
244 susceptibility to anesthetics and analgesics[2,17,36]. These complications are most
245 noticeable during surgical procedures wherein DM1 patients exhibit much longer recovery
246 times from various anesthetics and muscle relaxants. In the case of a few anesthetics,
247 the patient may require intervention to prevent death[18,37]. Because the liver is the primary
248 organ involved in drug metabolism, we hypothesized that DM1 livers might be
249 compromised in responding to and metabolizing xenobiotics, thereby decreasing DM1
250 patients' ability to clear certain drugs from their system.
251 We first chose zoxazolamine, a muscle relaxant, to test this hypothesis.
252 Zoxazolamine testing in mice consists of inducing muscle paralysis in the animals via
253 zoxazolamine injection and then monitoring them until they can self-right and move
254 around freely (Fig. 4a). Zoxazolamine metabolism shows a sex-specific response in mice;
255 however, in both males and females, DM1 mice took at least 50% longer to recover from
256 the drug-induced paralysis (Fig. 4b).
257 We next tested if a similar reduction in drug metabolism occurred with common,
258 over-the-counter analgesics such as acetaminophen (APAP). APAP causes severe liver
259 injury/damage if consumed in high concentrations as it generates toxic levels of N-acetyl-
260 p-benzoquinone imine (NAPQI) metabolite after oxidation by CYP2E1 in perivenous

hepatocytes[38] (Fig. 4c). Even a low dose of APAP can induce liver toxicity if CYP2E1 activity is high. Conversely, the liver can be insulated from APAP toxicity if CYP2E1 activity is ablated[39]. In most mice strains, the LD50 of APAP is between 320 and 370 mg per kg of body weight when administered intraperitoneally[40]. To see if DM1 changed susceptibility to APAP-induced hepatic injury, we injected 350 mg of APAP per kg of body weight into fasted DM1 and control mice. Mice were monitored for 8 hours and left to recover for 16 hours before being sacrificed.

A difference was immediately noticed between DM1 and control mice, as significantly more control mice died within the first 8 hours compared to DM1 mice (Fig. 4d). Upon collecting the liver from the surviving mice, 24 hours post-APAP injection, almost all control animals show widespread signs of liver necrosis (Fig. 4e). However, APAP-treated DM1 livers showed fewer instances of injury and necrosis. H&E staining of the APAP-treated livers also showed marked differences between DM1 and control mice, with DM1 mice still showing extensive injury and hepatocyte vacuolization but far less necrosis (Fig. 4f). Western blot analysis of cytochrome P450 2E1 (CYP2E1), a key enzyme involved in the metabolism APAP into NAPQI[38,41], showed that CYP2E1 is expressed at significantly lower levels in the livers of DM1 afflicted mice (Fig. 4g). Similarly, sulfotransferase 2a1 (SULT2a1), an enzyme associated with phase 2 drug metabolism[42,43], was also downregulated in the livers of the DM1 mice.

DM1 murine liver models are more susceptible to fatty liver disease and injury

As DM1 patients face dietary and mobility challenges that often require counseling and careful monitoring, we set out to test if the macronutrient composition of the patient's

diet impacts the DM1 liver's susceptibility to NAFLD[2,4,44,45]. To do so, we fed DM1 liver mice, and ApoE-rtTA controls standard chow supplemented with a 2 g/kg Dox diet until weaning, as previously described. Once weaned, the mice were switched to a high-fat, high-sugar, and heightened cholesterol (western) diet supplemented with 0.1 g/kg Dox for eight additional weeks (Fig. 5a)[46,47]. As before, we analyzed GTT and four-hour fasting glucose levels before sacrifice.

GTT analysis again showed no difference between DM1 mice and control animals (Fig. 5b); however, there was a slight difference in 4-hour fasted blood glucose levels between male DM1 and male control mice (Fig. 5c). In reverse of the basal diet, DM1 mice had significantly lower blood glucose.

While control livers turned pale following a high fat, high sugar diet, the DM1 livers became exceedingly lighter, with much of the usual red color replaced with off-white due to excess lipid accumulation (Fig 5d). Both DM1 and control mice showed significant increases in micro-and macro-vesicular steatosis, inflammation, and evidence of cell death on the western diet compared to the regular chow diet (Fig. 5e). However, DM1 mice showed more macro-vesicular steatosis and patchy necrosis as well as ballooning and feathery degeneration after western diet feeding.

Oil Red O staining showed that livers of DM1 mice had a much higher density of lipid droplets and a significant increase in the number of large lipid droplets (Fig. 5e), making them challenging to quantify via image analysis. Therefore, we used an alternative method to determine the relative accumulation of lipids in the western diet-fed control and DM1 mice. A hexane/isopropanol lipid extraction protocol collected hydrophobic fatty acids from small liver portions. A colorimetric assay for triglycerides was

307 performed on these extracts (Fig. 5f). This analysis revealed two features. First, the livers
308 from DM1 mice fed the regular rodent diet accumulated as many triglycerides as those
309 from control mice on the western diet. Second, the livers of DM1 mice fed a western diet
310 accumulated significantly more triglycerides than any other group.

311 Western diet-fed DM1 mice also had a more significant increase in the liver-to-
312 body weight ratios than controls (Fig. 5g). The mean body weight between DM1 and
313 control mice is invariant, suggesting that the increased accumulation of lipids in the liver
314 is not due to a more significant increase in body weight (Supplementary Fig. 2e).

315

316 **Upregulation of an alternatively spliced ACC1 isoform drives lipid accumulation in**
317 **DM1 liver**

318 To investigate how DM1 affects liver-specific lipid handling/metabolism and leads
319 to a fatty liver, we focused on DM1-related changes in splicing/abundance of transcripts
320 linked to lipogenesis, lipid transport, lipid metabolism, and NAFLD. Of these, acetyl-CoA
321 carboxylase 1 (*Acc1*) particularly stood out (Fig. 6a). ACC1 is at the rate-limiting step for
322 the conversion of excess citrate into free fatty acids (Fig. 6b); thus, any changes in its
323 function or regulation could directly lead to excess lipid production and potentially explain
324 the steatosis noted in the DM1-afflicted livers. ACC1 regulation involves multiple
325 phosphorylation clusters and a necessary dimerization event to function[48–53]. Upon
326 activation, ACC1 converts acetyl-CoA to malonyl-CoA, a necessary building block for fatty
327 acid synthesis and lipogenesis. ACC1 activity is negatively regulated through
328 phosphorylation by the kinases AMPK, PKA, and CDK and by excess palmitoyl-CoA

329 levels. In contrast, it is positively regulated by insulin-induced dephosphorylation via the
330 phosphatase PP2A and excess citrate levels (Fig. 6b)[54–56].

331 The exon 28 that changes in the context of DM1 is centrally situated in the protein-
332 coding region of the *Acc1* transcript; exclusion of the exon results in the loss of 24 amino
333 acids directly N-terminal to the central phosphorylation cluster (Fig. 6c)[55,57]. This exon is
334 included in *Acc1* transcripts in most tissues, having only been demonstrated to be
335 excluded in the brain, mammary tissues, ovaries, and liver[57]. In mammary tissues of
336 sheep and goats, skipping of this exon results in increased phosphorylation and
337 decreased function of ACC1, altering the lipid profiles of ovine milk[57,58].

338 In the livers of DM1 mice, exon 28 was included in ~30% more *Acc1* transcripts
339 than in control mice (Fig. 6a, d). Unexpectedly, MBNL1 deficiency in the liver did not affect
340 *Acc1* splicing (Fig. 6a). Furthermore, upon feeding a high-fat, high-sugar diet, the
341 inclusion of exon 28 increased slightly in control but not in DM1 mice, which maintained
342 similar PSI values as on standard chow (Fig. 6d). Additionally, western blot analysis
343 showed significantly higher ACC1 protein levels in the livers of DM1 mice relative to
344 controls (Fig. 6e). Whether increased ACC1 protein abundance in DM1 mice livers is
345 linked to exon 28 inclusion or occurred independently through another event regulating
346 translation or protein stability remains to be determined.

347 To discern whether the upregulation of alternatively spliced ACC1 isoform was a
348 primary consequence of DM1 or a secondary response to steatosis, we used an acute
349 DM1 liver model. In contrast to the chronic model, “acute DM1” mice were aged for eight
350 weeks before being fed 0.1g/kg Dox-containing diet for 12 days (Supplementary Fig. 3a).
351 The acute DM1 mice did not exhibit any steatosis, which was evident in the chronic DM1

model (Fig. 6f). Next, we compared the hepatic mRNA abundance of genes that are directly linked to lipid biosynthesis, transport or metabolism-related functions in acute versus chronic DM1 mice via qPCR. In many cases, the mRNA levels were similar between acute and chronic DM1 livers. However, some transcripts in the acute model showed significant differences in the chronic model, highlighting transcripts that may have changed in response to pathological changes in the chronic DM1 liver (Fig. 6g, Supplementary Fig. 3b, c). Importantly, missplicing of *Acc1*, *Pnpla6*, and *Sorbs1* transcripts was evident in both acute and chronic DM1 liver models (Fig. 6h; Supplementary Fig. 3d). Acute DM1 livers also demonstrated significant increase in ACC1 protein levels; but, this increase was lower than in chronic DM1 livers (Supplementary Fig. 3b). These data demonstrate that ACC1 misregulation in DM1 is a direct effect of repeat RNA toxicity and not a secondary response to lipid accumulation or liver injury.

To determine if the upregulation of alternatively spliced ACC1 isoform contributes to DM1-related NAFLD, chronic DM1 mice were treated with antisense oligonucleotides (ASO) targeting the 5'ss of exon 28 of *Acc1* (Supplementary Fig. 3f). ASO treatment consisted of two loading doses of 12 mg/kg ASO the first two days of treatment, followed by two maintenance doses on days six and ten, and the mice were sacrificed on day eleven. After ASO treatment, the inclusion of exon 28 in DM1 mice livers dropped to less than 20%, an almost 60% decrease relative to untreated or control ASO-treated DM1 livers (Fig. 6i). Despite having a striking effect on *Acc1* splicing, the ASO treatment did not cause a noticeable change in ACC1 protein abundance (Supplementary Fig. 3e). These data indicate that increase in ACC1 and its splice isoform switch are likely two

separate events and that upregulation of ACC1 protein in DM1 is not a consequence of higher protein stability or increased mRNA translation of the alternative isoform. We next evaluated the functionality of *Acc1* splicing redirection on lipid accumulation in DM1 mice livers. Chronic DM1 mice treated with ASO targeting *Acc1* exon 28 showed only a modest improvement in hepatic steatosis compared to control ASO treatment (Fig. 6j).

To further investigate whether ACC1 is required for the development of NAFLD phenotype in DM1-afflicted mice livers, we used the ACC1 inhibitor (CP-641086) to prevent ACC1 activity in these mice (Supplementary Fig. 4b). This inhibitor has been previously characterized for its ability to inhibit ACC1 activity, and it effectively reduces malonyl-CoA concentrations and fatty acid synthesis in cultured cells and mice livers[59,60]. We orally administered 25 μg/g ACC1 inhibitor twice daily to chronic DM1 mice for five days and then analyzed their liver health. Strikingly, short-term inhibition of ACC1 activity led to a significant recovery in hepatic steatosis in DM1-afflicted livers (Fig. 6k, Supplementary Fig. 4c) without affecting the expression of most lipid metabolism-related genes (Fig. 6j; Supplementary Fig. 3c). However, while the inhibition of ACC1 significantly reduced the appearance of fatty liver, markers of poor liver health associated with DM1-related NAFLD, such as increased hepatosomatic index and lobular inflammation failed to improve after treatment (Supplementary Fig. 4d, e). This suggests that these phenotypes in chronic DM1 mice either occur independently of ACC1 dysregulation or that a longer-term ACC1 inhibition is required to reverse the pathologies developing from sustained lipid accumulation. Collectively, these data demonstrate that upregulation of the alternative ACC1 splice isoform drives the bulk of hepatic lipid accumulation in DM1

397 and that short-term inhibition of ACC1 can reverse the hepatic steatosis phenotype in
398 DM1-afflicted mice livers.

Discussion

DM1 symptoms often extend beyond the musculature, wherein various tissues manifest specific pathologies that contribute to the affected individual's overall health[10,26,61]. For instance, patients commonly experience gastrointestinal disturbances, metabolic dysregulation, increased sensitivity to drug injury, as well as the development of NAFLD and other liver dysfunctions[18–20,22,62–65]. However, the root cause of such dysfunctions is not fully understood. Elevated liver enzyme levels (GGT, AP) in DM1 individuals are also observed consistently but are speculated to occur secondary to the gallbladder and bile duct dysmotility, which might impair bile excretion and indirectly affect liver function[22,62]. In this study, we provide multiple lines of evidence that targeted expression of CUG repeat-containing RNA within hepatocytes is sufficient to alter the function of the liver, resulting in steatosis and hepatocellular injury. When combined with diet-induced metabolic stress, this predisposes the DM1 liver toward NAFLD and compromises its ability to respond to and metabolize specific analgesics and muscle relaxants. We determined that both NAFLD and poor drug metabolism phenotypes are direct consequences of repeat RNA toxicity in the liver, as these defects were not seen in the HSA L/R transgenic mice, which express repeat RNA only in the muscle tissues. Conversely, the HSA L/R mice suffer from significant glucose intolerance, whereas the DM1 liver mice are normal in glucose handling. These findings highlight the importance of studying the effects of DM1 within individual tissues and evaluating their respective contributions to the metabolic symptoms of this complex disease.

We further demonstrate that hepatic expression of toxic CUG960i RNA triggers global mRNA abundance and processing defects in genes enriched in ontologies that group into

major functional clusters, especially lipid and drug metabolism, cell signaling and immune responses, as well as macromolecular binding and transport-related activities. These gene expression defects can directly lead to increased lipid accumulation and heighten the liver's vulnerability to damage from toxins/dietary stress, partly explaining the high incidence of NAFLD and metabolic disorders seen in DM1 patients[19,20,22]. For instance, scores of genes involved in phase I and II drug metabolism were misregulated in the DM1 liver model. Notably, the levels of CYP2E1 and SULT2A1 proteins were significantly reduced in the livers of DM1 mice. A decrease in these two proteins alone may help to explain some of the poor responses to sedatives seen in DM1 patients, especially in the case of commonly inhaled anesthetics, which tend to be halogenated-hydrocarbons[66–68]. Further work is needed to determine whether abnormal drug metabolism or dysregulation of drug-metabolizing enzymes is a direct consequence of repeat RNA toxicity or an aberrant response to lipid accumulation and DM1-related NAFLD.

The pathological mechanism of DM1 involves sequestration and disruption of MBNL protein activities, shifting the affected tissues' transcriptome from an adult-to-preadolescent-like state. Also, MBNL expression is upregulated in hepatocytes as the liver matures after birth[69,70]. Intriguingly, when we compared the hepatic transcriptomes of DM1 and *Mbnl1* KO mice, less than a third of the misregulated events occurring in the DM1 hepatocytes were detected in MBNL1 deficient hepatocytes. The dissimilarities between the DM1 liver model and *Mbnl1* KOs were also evident at the tissue level, as many of the pathological consequences of expressing DM1 in the liver were not seen in the *Mbnl1* KO mice, including the lack of lipid accumulation. MBNL proteins serve critical functions in maintaining tissue maturity; however, which MBNL family member is

445 predominantly responsible for these activities is tissue-dependent[11,71–74]. Additionally,
446 MBNL proteins have high sequence and structure similarity and significant overlap in
447 binding targets; thus, substitution between the two predominant members, MBNL1 and
448 MBNL2, allows for a tunable regulatory system that maintains appropriate splicing form
449 for the bulk of co-regulated transcripts[73–75]. Our examination of *Mbnl1* KO mice revealed
450 that MBNL2 protein levels are increased in the KO livers, a phenomenon also seen in
451 other tissues[34,72,74,76]. In the future, it would be interesting to determine whether elevated
452 expression of MBNL2 could explain the lack of overlap in transcriptome changes between
453 the *Mbnl1* KO and DM1 livers, as well as shed light on possible compensatory
454 mechanism(s) that buffer the effects of MBNL1 loss within the liver.

455 Several genes associated with insulin-regulated lipid metabolism were altered in
456 DM1-afflicted livers. Because lipid homeostasis is regulated jointly by intra- and extra-
457 hepatic signaling, these changes could be a primary result of repeat RNA toxicity or a
458 secondary effect of the diseased liver. Indeed, there is some evidence of a secondary
459 effect occurring — the expression and/or splicing of genes such as *Sorbs1*, *Fabp1*,
460 *Acox1*, and *Hsd17b13* were altered less in the acute DM1 liver as compared to the chronic
461 DM1 liver, possibly indicating effects that are exacerbated with lipid accumulation.
462 However, based on our analysis, missplicing and upregulation of ACC1 is a rapid
463 response to the repeat RNA expression. ACC1 is a focal point for *de novo* lipid
464 biosynthesis, converting excess acetyl-CoA into malonyl-CoA, which can then be used to
465 produce palmitate[77,78]. Therefore, ACC1 activity must be tightly controlled in response to
466 the nutritional state of the liver as misregulation of ACC1 stimulates excess lipogenesis
467 and NAFLD phenotypes[79,80].

Our results indicate that short-term inhibition of ACC1 activity is sufficient to reverse lipid accumulation in the DM1-afflicted mice livers, highlighting the importance and involvement of this pathway. We believe this beneficial effect is primarily due to inhibition of *de novo* lipogenesis; however, reduced production of malonyl-CoA would also increase the mitochondrial import and oxidation of fatty acids. Although extrapolating these findings to DM1-related NAFLD in humans is not straightforward, pharmacologic inhibition of ACC is currently viewed as one of the most promising therapeutic approaches for treating NAFLD/NASH[81–85]. It is important to note that a small proportion of NAFLD patients treated with ACC inhibitors may experience hypertriglyceridemia over time, which can increase their risk of developing cardiovascular disease[86–88]. Whether inhibiting ACC1 in the context of DM1 leads to increased serum triglycerides remains to be determined. Therefore, in future studies, it will be essential to examine the long-term effects of ACC1 inhibitors on systemic lipid trafficking and mobilization in DM1 liver mice.

In conclusion, our study provides the first characterization of the direct impact of DM1 on liver health. The findings offer valuable insights into how disrupted hepatic functions contribute to the metabolic symptoms and drug sensitivities in DM1, underscoring the idea that a malfunctioning liver can further complicate the treatment of this complex genetic disease. A current limitation of this work is that our results need to be validated in humans, and the extent of similarity between the murine DM1 liver model and actual patient livers must be systematically assessed. Therefore, enhanced screening for NAFLD/hepatocellular injury in affected individuals, along with access to liver biopsies, is urgently needed because if DM1 livers cannot provide adequate metabolism of xenobiotic material, it would prolong the clearance time for many drugs,

491 altering their therapeutic index. Future investigations incorporating patient samples and
492 combining clinical data with the mouse model findings will be pivotal in determining the
493 extent of hepatic dysfunctions in DM1. This will help ensure the applicability, optimization,
494 and effectiveness of prospective treatments being developed to treat/manage various
495 symptoms of this debilitating disease.

Methods

Development of the DM1 Liver Model.

The "DM1 liver" line was generated by crossbreeding TRE-960i mice with ApoE-rtTA mice. ApoE-rtTA mice express a reverse tetracycline transactivator (rtTA) under a liver-specific ApoE promoter[89]. TRE-960i mice carry a tetracycline response element (TRE)-driven truncated DMPK gene with a $(CUG)_{960}$ repeat sequence in the final exon[23]. Mice with ApoE-rtTA alone were used as controls. Both lines were maintained as homozygotes for transgenic alleles. Mouse care and use followed NIH guidelines for animal care, and animal protocols were approved by the Institutional Animal Care and Use Committee at the University of Illinois at Urbana-Champaign.

Mouse diet schemes.

In most experiments, DM1 liver and ApoE-rtTA mice were subjected to the disease-inducing Dox diet from birth, with mothers receiving 2.0 g/kg Dox-supplemented Teklad 2018 18% protein global rodent diet until weaning at 21 days. Subsequently, weaned mice transitioned to a 0.1 g/kg Dox diet until sacrifice at nine weeks. This feeding protocol is referred to as the chronic DM1 liver model.

Exceptions to the protocol above include: DM1 liver mice used for RNA-seq, which remained on a 2 g/kg Dox diet until sacrifice. "No-Dox" mice were ApoE-rtTA; TRE960i mice maintained on a Dox-free diet. "Recovery" mice followed the chronic DM1 protocol but were transitioned to a Dox-free diet for ten days before sacrifice. For the Western Diet model, mothers were on 2g/kg Dox-supplemented chow until weaning. Then, mice were switched to a high-fat, high-sugar, cholesterol-supplemented "Western" diet (Teklad 88137) supplemented

with 0.1g/kg Dox for eight weeks. In the acute DM1 model, mice were Dox-free until eight weeks, followed by a 0.1 g/kg Dox diet for 12 or 18 days before sacrifice.

Zoxazolamine recovery testing.

Zoxazolamine (Zox) solution, prepared the day before, consisted of Zox dissolved in DMSO to achieve a final concentration of 15 µg/µL in a 95% Corn-Oil, 5% DMSO solution. After an 18-22 hour fast, mice received 120 mg/kg Zox injections. Vigorous homogenization between injections ensured a uniform solution. Post-treatment, mice freely roamed until they lost motor function, after which they were placed supine on an insulating blanket. Time was recorded until mice successfully self-righted three times[90].

APAP insult testing.

Acetaminophen (APAP) solutions were freshly prepared, dissolving 20 mg of APAP in 1 mL sterile 1x PBS. After heating at 55°C for 15 minutes with periodic vortexing, the solution was maintained at 40°C during injection, with thorough mixing between injections. Mice fasted for 18-22 hours and received a 350 mg/kg IP injection of APAP. Mice were observed for 8 hours when surviving mice returned to the animal care facility. Harvesting of serum and liver samples occurred 24 hours post-APAP injection[91,92].

***Acc*1 exon 28 ASO treatment.**

Acc1 Exon 28 ASO, developed by Gene Tools, LLC, targeted the 5' splicing site of *Acc1* exon 28 (sequence: CCCTCTGTAATTAAA). A standard control in-vivo morpholino with the sequence CCTCTTACCTCAGTT served as a control. ASOs were dissolved in sterile biology-grade water. Mice designated for ASO treatment followed the chronic DM1 model until day 63,

receiving IP injections of 12 mg ASO per kg body weight on days 63, 64, 68, and 72. Mice were sacrificed after a 4-6 hour fast on day 73.

ACC1 inhibitor treatment.

ACC1 inhibitor CP-641086, procured from MedChemExpress (Lot#12439), was dissolved in a 5% (w/w) methylcellulose solution in molecular biology-grade water. Mice selected for ACC1 inhibitor treatment followed the chronic DM1 model until day 63. They received doses of either 25 µg inhibitor or vehicle (5% methylcellulose) per g body weight twice daily via oral gavage for five days. Sacrifice occurred on the sixth day after 4-6 hours of fasting.

Statistical analysis and data visualization.

All quantitative experiments have at least three independent biological repeats. The results were expressed with mean and standard deviation unless mentioned otherwise. Differences between groups were examined for statistical significance using unpaired T-tests when comparing directly between groups or one-way analysis of variance (ANOVA) for more than two groups using the GraphPad Prism 9 Software. Statistical outliers were determined with the ROUT method in Prism, with Q = 5%. P-value < 0.05 or FDR < 0.10 was considered significant. RNA-seq data plots were generated in R using the ggplot2 package. In all figures, significance was set as $p < 0.05$, "*" indicates $p < 0.05$, "**" indicates $p < 0.01$, "***" indicates $p < 0.001$, and "****" indicates $p < 0.0001$. Data presented as bar graph or linear For Box plots: median is represented as center line, median; box limits are the upper and lower quartiles; whiskers are set as 1.5x interquartile range.

RESOURCE AVAILABILITY

Data Availability

RNA-Seq data that support the findings of this study have been deposited in NCBI Gene Expression Omnibus under the primary accession code GSE252827 (https://www.ncbi.nlm.nih.gov/geo/query/acc.cgi?acc=GSE252827)

Materials Availability

Requests for reagents, resources, and additional information should be directed to the corresponding author, Auinash Kalsotra (kalsotra@illinois.edu).

References

1. Harper, P. S. *Myotonic Dystrophy*. (W.B. Saunders, 2003).
2. Ashizawa, T. *et al.* Consensus-based care recommendations for adults with myotonic dystrophy type 1. *Neurol. Clin. Pract.* **8**, 507–520 (2018).
3. Johnson, N. E. *et al.* Population Based Prevalence of Myotonic Dystrophy Type 1 Using Genetic Analysis of State-wide Blood Screening Program. *Neurology* 10.1212/WNL.000 (2021) doi:10.1212/wnl.0000000000011425.
4. Heatwole, C. *et al.* Patient-reported impact of symptoms in myotonic dystrophy type 1 (PRISM-1). *Neurology* **79**, 348–357 (2012).
5. Day, J. W. & Ranum, L. P. W. Genetics and molecular pathogenesis of the myotonic dystrophies. *Curr. Neurol. Neurosci. Rep.* **5**, 55–60 (2005).
6. Brook, J. D. *et al.* Molecular basis of myotonic dystrophy: Expansion of a trinucleotide (CTG) repeat at the 3′ end of a transcript encoding a protein kinase family member. **68**, 799–808 (1992).
7. Lee, J. E. & Cooper, T. A. Pathogenic mechanisms of myotonic dystrophy. *Biochem. Soc. Trans.* **37**, 1281–1286 (2009).
8. Mankodi, A. Myotonic Dystrophy in Transgenic Mice Expressing an Expanded CUG Repeat. **289**, 1769–1772 (2000).
9. Miller, J. W. *et al.* Recruitment of human muscleblind proteins to (CUG)n expansions associated with myotonic dystrophy. *EMBO J.* **19**, 4439–4448 (2002).
10. Jiang, H., Mankodi, A., Swanson, M. S., Moxley, R. T. & Thornton, C. A. Myotonic dystrophy type 1 is associated with nuclear foci of mutant RNA, sequestration of muscleblind proteins and deregulated alternative splicing in neurons. *Hum. Mol. Genet.* **13**, 3079–3088 (2004).
11. Wang, E. T. *et al.* Transcriptome-wide regulation of pre-mRNA splicing and mRNA localization by muscleblind proteins. *Cell* **150**, 710–724 (2012).
12. Lin, X. *et al.* Failure of MBNL1-dependent post-natal splicing transitions in myotonic dystrophy. *Hum. Mol. Genet.* **15**, 2087–2097 (2006).
13. Chau, A. & Kalsotra, A. Developmental insights into the pathology of and therapeutic strategies for DM1: Back to the basics. *Dev. Dyn.* **244**, 377–390 (2015).
14. Ho, T. H. *et al.* Muscleblind proteins regulate alternative splicing. *EMBO J.* **23**, 3103–3112 (2004).
15. Philips, A. V., Timchenko, L. T. & Cooper, T. A. Disruption of Splicing Regulated by a CUG-Binding Protein in Myotonic Dystrophy. *Science (80-.).* **280**, 737–741 (1998).

16. Yum, K., Wang, E. T. & Kalsotra, A. Myotonic dystrophy: disease repeat range, penetrance, age of onset, and relationship between repeat size and phenotypes. *Curr. Opin. Genet. Dev.* **44**, 30–37 (2017).

17. Campbell, N., Brandom, B., Day, J. W. & Moxley, R. Practical Suggestions for the Anesthetic Management of a Myotonic Dystrophy Patient FOREWORD : **1**, 1–6 (2010).

18. Mathieu, J. *et al.* Anesthetic and surgical complications in 219 cases of myotonic dystrophy. *Neurology* **49**, 1646 LP – 1650 (1997).

19. Bhardwaj, R. R. & Duchini, A. Non-alcoholic steatohepatitis in myotonic dystrophy: DMPK gene mutation, insulin resistance and development of steatohepatitis. *Case Rep. Gastroenterol.* **4**, 100–103 (2010).

20. Shieh, K., Gilchrist, J. M. & Promrat, K. Frequency and predictors of nonalcoholic fatty liver disease in myotonic dystrophy. *Muscle and Nerve* **41**, 197–201 (2010).

21. John Herbick, C. J. Hepatic Glycogenosis in a Patient with Type 1 Myotonic Dystrophy. *J. Liver Dis. Transplant.* **02**, 2012–2014 (2013).

22. Achiron, A. *et al.* Abnormal liver test results in myotonic dystrophy. *J. Clin. Gastroenterol.* **26**, 292–295 (1998).

23. Morriss, G. R., Rajapakshe, K., Huang, S., Coarfa, C. & Cooper, T. A. Mechanisms of skeletal muscle wasting in a mouse model for myotonic dystrophy type 1. *Hum. Mol. Genet.* **27**, 2789–2804 (2018).

24. Dong, J. *et al.* Elucidation of a Universal Size-Control Mechanism in Drosophila and Mammals. *Cell* **130**, 1120–1133 (2007).

25. Lee, J. *et al.* Intrinsically cell-penetrating multivalent and multitargeting ligands for myotonic dystrophy type 1. *Proc. Natl. Acad. Sci.* **116**, 8709–8714 (2019).

26. Machuca-Tzili, L., Brook, D. & Hilton-Jones, D. Clinical and molecular aspects of the myotonic dystrophies: A review. *Muscle Nerve* **32**, 1–18 (2005).

27. Wheeler, T. M. & Thornton, C. A. Myotonic dystrophy: RNA-mediated muscle disease. *Curr. Opin. Neurol.* **20**, 572–576 (2007).

28. Scotti, M. M. & Swanson, M. S. RNA mis-splicing in disease. *Nat. Rev. Genet.* **17**, 19–32 (2016).

29. Huang, D. W., Sherman, B. T. & Lempicki, R. A. Systematic and integrative analysis of large gene lists using DAVID bioinformatics resources. *Nat. Protoc.* **4**, 44–57 (2009).

30. Sobczak, K. *et al.* Loss of MBNL Leads to Disruption of Developmentally Regulated Alternative Polyadenylation in RNA-Mediated Disease. *Mol. Cell* **56**, 311–322 (2014).

31. Wang, E. T. *et al.* Transcriptome alterations in myotonic dystrophy skeletal muscle and heart. *Hum. Mol. Genet.* **28**, 1312–1321 (2019).

651 32. Kanadia, R. N. *et al.* A Muscleblind Knockout Model for Myotonic Dystrophy.
652 *Science (80-.).* **302**, 1978–1980 (2003).

653 33. Bangru, S. *et al.* Alternative splicing rewires Hippo signaling pathway in
654 hepatocytes to promote liver regeneration. *Nat. Struct. Mol. Biol.* **25**, 928–939
655 (2018).

656 34. Nitschke, L., Hu, R.-C., Miller, A. N., Lucas, L. & Cooper, T. A. Alternative splicing
657 mediates the compensatory upregulation of MBNL2 upon MBNL1 loss-of-function.
658 *Nucleic Acids Res.* gkac1219 (2023) doi:10.1093/nar/gkac1219.

659 35. Rogalska, Z. & Sobczak, K. Sustainable recovery of MBNL activity in
660 autoregulatory feedback loop in myotonic dystrophy. *Mol. Ther. - Nucleic Acids*
661 **30**, 438–448 (2022).

662 36. Veyckemans, F. & Scholtes, J. L. Myotonic DYSTROPHIES type 1 and 2:
663 Anesthetic care. *Paediatr. Anaesth.* **23**, 794–803 (2013).

664 37. Groh, W. J. *et al.* Electrocardiographic Abnormalities and Sudden Death in
665 Myotonic Dystrophy Type 1. *N. Engl. J. Med.* **358**, 2688–2697 (2008).

666 38. James, L. P., Mayeux, P. R. & Hinson, J. A. Acetaminophen-induced
667 hepatotoxicity. *Drug Metabolism and Disposition* (2003)
668 doi:10.1124/dmd.31.12.1499.

669 39. Zaher, H. *et al.* Protection against Acetaminophen Toxicity in CYP1A2 and
670 CYP2E1 Double-Null Mice. *Toxicol. Appl. Pharmacol.* **152**, 193–199 (1998).

671 40. Mcclain, C. J. Potentiation of Acetaminophen Hepatotoxicity by Alcohol. *JAMA J.*
672 *Am. Med. Assoc.* **244**, 251 (1980).

673 41. Bao, Y. *et al.* Alterations of Cytochrome P450–Mediated Drug Metabolism during
674 Liver Repair and Regeneration after Acetaminophen-Induced Liver Injury in
675 MiceS. *Drug Metab. Dispos.* **50**, 694–703 (2022).

676 42. Senggunprai, L., Yoshinari, K. & Yamazoe, Y. Selective Role of Sulfotransferase
677 2A1 (SULT2A1) in the N-Sulfoconjugation of Quinolone
678 Drugs in Humans. *Drug Metab. Dispos.* **37**, 1711 LP – 1717 (2009).

679 43. Gamage, N. *et al.* Human Sulfotransferases and Their Role in Chemical
680 Metabolism. *Toxicol. Sci.* **90**, 5–22 (2006).

681 44. Turner, C. & Hilton-Jones, D. The myotonic dystrophies: Diagnosis and
682 management. *J. Neurol. Neurosurg. Psychiatry* **81**, 358–367 (2010).

683 45. Savkur, R. S., Philips, A. V & Cooper, T. A. Aberrant regulation of insulin receptor
684 alternative splicing is associated with insulin resistance in myotonic dystrophy.
685 *Nat. Genet.* **29**, 40–47 (2001).

686 46. Escolà-Gil, J. C. *et al.* The cholesterol content of western diets plays a major role
687 in the paradoxical increase in high-density lipoprotein cholesterol and upregulates
688 the macrophage reverse cholesterol transport pathway. *Arterioscler. Thromb.*

Vasc. Biol. **31**, 2493–2499 (2011).

47. Elmgren, A. *et al.* Acutely reduced locomotor activity is a major contributor to Western diet-induced obesity in mice. *Am. J. Physiol. Metab.* **294**, E251–E260 (2007).

48. Ha, J., Daniel, S., Broyles, S. S. & Kim, K. H. Critical phosphorylation sites for acetyl-CoA carboxylase activity. *J. Biol. Chem.* **269**, 22162–22168 (1994).

49. Halestrap, A. P. & Denton, R. M. Hormonal regulation of adipose-tissue acetyl-coenzyme A carboxylase by changes in the polymeric state of the enzyme. The role of long-chain fatty acyl-coenzyme A thioesters and citrate. *Biochem. J.* **142**, 365–377 (1974).

50. Hunkeler, M. *et al.* Structural basis for regulation of human acetyl-CoA carboxylase. *Nature* **558**, 470–474 (2018).

51. Munday, M. R., Campbell, D. G., Carling, D. & Hardie, D. G. Identification by amino acid sequencing of three major regulatory phosphorylation sites on rat acetyl-CoA carboxylase. *Eur. J. Biochem.* **175**, 331–338 (1988).

52. Wei, J. *et al.* A unified molecular mechanism for the regulation of acetyl-CoA carboxylase by phosphorylation. *Cell Discov.* **2**, 16044 (2016).

53. Witters, L. A., Kowaloff, E. M. & Avruch, J. Glucagon regulation of protein phosphorylation. Identification of acetyl coenzyme A carboxylase as a substrate. *J. Biol. Chem.* **254**, 245–248 (1979).

54. Davies, S. P., Sim, A. T. R. & Hardie, D. G. Location and function of three sites phosphorylated on rat acetyl-CoA carboxylase by the AMP-activated protein kinase. *Eur. J. Biochem.* **187**, 183–190 (1990).

55. Kong, I. S., López-Casillas, F. & Kim, K. H. Acetyl-CoA carboxylase mRNA species with or without inhibitory coding sequence for Ser-1200 phosphorylation. *J. Biol. Chem.* **265**, 13695–13701 (1990).

56. Winder, W. W. *et al.* Phosphorylation of rat muscle acetyl-CoA carboxylase by AMP-activated protein kinase and protein kinase A. *J. Appl. Physiol.* **82**, 219–225 (1997).

57. Barber, M., Pooley, L. & Travers, M. Developmental regulation of alternatively spliced acetyl-CoA carboxylase-alpha mRNAs encoding isozymes with or without an eight amino acid domain upstream of the Ser-1200 phosphorylation motif in the mammary gland. *J. Mol. Endocrinol.* **27**, 349–356 (2001).

58. Badaoui, B. *et al.* Goat Acetyl-Coenzyme A Carboxylase α: Molecular Characterization, Polymorphism, and Association with Milk Traits. *J. Dairy Sci.* **90**, 1039–1043 (2007).

59. Harwood, H. J. J. *et al.* Isozyme-nonselective N-Substituted Bipiperidylcarboxamide Acetyl-CoA Carboxylase Inhibitors Reduce Tissue Malonyl-CoA Concentrations, Inhibit Fatty Acid Synthesis, and Increase Fatty

Acid Oxidation in Cultured Cells and in Experimental Animals. *J. Biol. Chem.* **278**, 37099–37111 (2003).

60. Zhang, H., Tweel, B., Li, J. & Tong, L. Crystal Structure of the Carboxyltransferase Domain of Acetyl-Coenzyme A Carboxylase in Complex with CP-640186. *Structure* **12**, 1683–1691 (2004).

61. Du, H. *et al.* Aberrant alternative splicing and extracellular matrix gene expression in mouse models of myotonic dystrophy. *Nat. Struct. Mol. Biol.* **17**, 187–193 (2010).

62. Perna, A. *et al.* High Prevalence and Gender-Related Differences of Gastrointestinal Manifestations in a Cohort of DM1 Patients: A Perspective, Cross-Sectional Study. *Front. Neurol.* **11**, 394 (2020).

63. Miele, L. *et al.* Clinical characteristics of metabolic associated fatty liver disease (MAFLD) in subjects with myotonic dystrophy type 1 (DM1). *Dig. liver Dis. Off. J. Ital. Soc. Gastroenterol. Ital. Assoc. Study Liver* **53**, 1451–1457 (2021).

64. Tanaka, N. *et al.* Non-alcoholic fatty liver disease later diagnosed as myotonic dystrophy. *World journal of hepatology* vol. 12 685–692 (2020).

65. Hama, M. *et al.* Metabolic complications in myotonic dystrophy type 1: A cross-sectional survey using the National Registry of Japan. *J. Neurol. Sci.* **427**, 117511 (2021).

66. Peter, R. *et al.* Hydroxylation of chlorzoxazone as a specific probe for human liver cytochrome P-450IIE1. *Chem. Res. Toxicol.* **3**, 566–573 (1990).

67. Spracklin, D. K., Hankins, D. C., Fisher, J. M., Thummel, K. E. & Kharasch, E. D. Cytochrome P450 2E1 is the principal catalyst of human oxidative halothane metabolism in vitro. *J. Pharmacol. Exp. Ther.* **281**, 400–411 (1997).

68. Gupta, N., N Saxena, K., Kumar Panda, A., Anand, R. & Mishra, A. Myotonic dystrophy: an anaesthetic dilemma. *Indian J. Anaesth.* **53**, 688–691 (2009).

69. Bhate, A. *et al.* ESRP2 controls an adult splicing programme in hepatocytes to support postnatal liver maturation. **6**, 8768 (2015).

70. Konieczny, P., Stepniak-Konieczna, E. & Sobczak, K. MBNL proteins and their target RNAs, interaction and splicing regulation. *Nucleic Acids Res.* **42**, 10873–10887 (2014).

71. Johnson, J. M. *et al.* A postnatal switch of CELF and MBNL proteins reprograms alternative splicing in the developing heart. *Proc. Natl. Acad. Sci.* **105**, 20333–20338 (2008).

72. Lee, K.-Y. *et al.* Compound loss of muscleblind-like function in myotonic dystrophy. *EMBO Mol. Med.* **5**, 1887–1900 (2013).

73. Lee, S. R., Pratt, G. A., Martinez, F. J., Yeo, G. W. & Lykke-Andersen, J. Target Discrimination in Nonsense-Mediated mRNA Decay Requires Upf1 ATPase

766 Activity. *Mol. Cell* **59**, 413–425 (2015).

767 74. Konieczny, P., Stepniak-Konieczna, E. & Sobczak, K. MBNL proteins and their
768 target RNAs, interaction and splicing regulation. *Nucleic Acids Res.* **42**, 10873–
769 10887 (2014).

770 75. Sznajder, Ł. J. *et al.* Mechanistic determinants of MBNL activity. *Nucleic Acids*
771 *Res.* **44**, gkw915 (2016).

772 76. Konieczny, P., Stepniak-Konieczna, E. & Sobczak, K. MBNL expression in
773 autoregulatory feedback loops. *RNA Biol.* **15**, 1–8 (2018).

774 77. Fullerton, M. D. *et al.* Single phosphorylation sites in Acc1 and Acc2 regulate lipid
775 homeostasis and the insulin-sensitizing effects of metformin. *Nat. Med.* **19**, 1649–
776 1654 (2013).

777 78. Thampy, K. G. & Wakil, S. J. Regulation of acetyl-coenzyme A carboxylase. I.
778 Purification and properties of two forms of acetyl-coenzyme A carboxylase from
779 rat liver. *J. Biol. Chem.* **263**, 6447–6453 (1988).

780 79. Softic, S. *et al.* Divergent effects of glucose and fructose on hepatic lipogenesis
781 and insulin signaling. *J. Clin. Invest.* **127**, 4059–4074 (2017).

782 80. Mao, J. *et al.* Liver-specific deletion of acetyl-CoA carboxylase 1 reduces hepatic
783 triglyceride accumulation without affecting glucose homeostasis. *Proc. Natl. Acad.*
784 *Sci.* **103**, 8552–8557 (2006).

785 81. Goedeke, L. *et al.* Acetyl-CoA Carboxylase Inhibition Reverses NAFLD and
786 Hepatic Insulin Resistance but Promotes Hypertriglyceridemia in Rodents.
787 *Hepatology* **68**, 2197–2211 (2018).

788 82. Tamura, Y. O. *et al.* Selective acetyl-CoA carboxylase 1 inhibitor improves hepatic
789 steatosis and hepatic fibrosis in a preclinical nonalcoholic steatohepatitis model.
790 *J. Pharmacol. Exp. Ther.* **379**, 280–289 (2021).

791 83. Zhang, X.-J., Cai, J. & Li, H. Targeting ACC for NASH resolution. *Trends Mol.*
792 *Med.* **28**, 5–7 (2022).

793 84. Zhang, X.-J. *et al.* A small molecule targeting ALOX12-ACC1 ameliorates
794 nonalcoholic steatohepatitis in mice and macaques. *Sci. Transl. Med.* **13**,
795 eabg8116 (2021).

796 85. Bian, H., Liu, Y.-M. & Chen, Z.-N. New avenues for NASH therapy by targeting
797 ACC. *Cell Metab.* **34**, 191–193 (2022).

798 86. Kim, C.-W. *et al.* Acetyl CoA Carboxylase Inhibition Reduces Hepatic Steatosis
799 but Elevates Plasma Triglycerides in Mice and Humans: A Bedside to Bench
800 Investigation. *Cell Metab.* **26**, 576 (2017).

801 87. Calle, R. A. *et al.* ACC inhibitor alone or co-administered with a DGAT2 inhibitor in
802 patients with non-alcoholic fatty liver disease: two parallel, placebo-controlled,
803 randomized phase 2a trials. *Nat. Med.* **27**, 1836–1848 (2021).

804 88. Loomba, R. *et al.* GS-0976 Reduces Hepatic Steatosis and Fibrosis Markers in
805 Patients With Nonalcoholic Fatty Liver Disease. *Gastroenterology* **155**, 1463-
806 1473.e6 (2018).

807 89. Xu, K. *et al.* Generation of the regulatory protein rtTA transgenic mice. *World J.*
808 *Gastroenterol.* **11**, 2885–2891 (2005).

809 90. Fujii, K., Jaffe, H. & Epstein, S. S. Factors influencing the hexobarbital sleeping
810 time and zoxazolamine paralysis time in mice. *Toxicol. Appl. Pharmacol.* **13**, 431–
811 438 (1968).

812 91. Mcgill, M. R., Williams, C. D., Xie, Y., Ramachandran, A. & Jaeschke, H.
813 Acetaminophen-induced liver injury in rats and mice: Comparison of protein
814 adducts, mitochondrial dysfunction, and oxidative stress in the mechanism of
815 toxicity. *Toxicol. Appl. Pharmacol.* **264**, 387–394 (2012).

816 92. Mossanen, J. & Tacke, F. Acetaminophen-induced acute liver injury in mice. *Lab.*
817 *Anim.* (2015) doi:10.1177/0023677215570992.

818

819 **Acknowledgments:** We acknowledge support from the Transgenic mouse core, High-
820 throughput sequencing and genotyping core, and Histology-microscopy core facilities at
821 the University of Illinois, Urbana-Champaign. We thank the members of the Kalsotra and
822 Anakk laboratories for their valuable discussions and comments on the manuscript.

823 **Author Contributions Statement:** Z.D. and A.K. conceived the project and designed the
824 experiments. Z.D. and A.G. performed experiments and analyzed the data. Z.D., AK, and
825 U.V.C facilitated mouse model development and management. Z.D. and A.K. interpreted
826 the results and wrote the manuscript. All authors discussed the results and edited the
827 manuscript.

828 **Competing Interests Statement:** The authors declare no competing financial interests.

829 **Funding sources:** Work in the Kalsotra laboratory is supported by the National Institute
830 of Health (R01HL126845, R01AA010154), the Muscular Dystrophy Association
831 (MDA514335), and the Beckman Fellowship from the Center for Advanced Study at the
832 University of Illinois Urbana-Champaign. Z.D. was supported by the NIH Chemistry–
833 Biology Interface training program (T32-GM070421). A.G. was supported by the Jenner
834 Family Summer Research Fellowship.

835

836 **Figures and Tables**

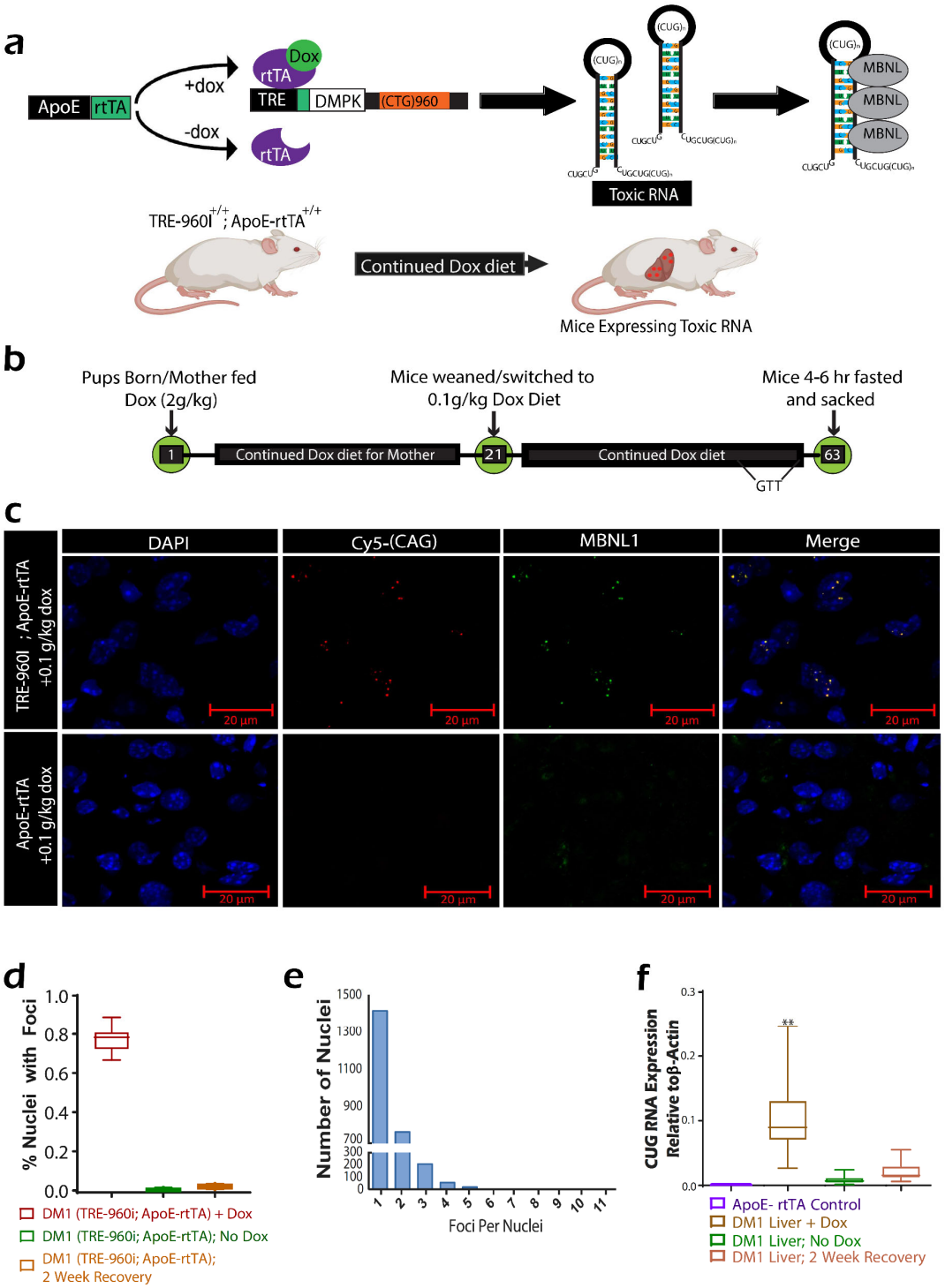

837

838 **Fig. 1. Murine Model Recapitulates Molecular Mechanism of DM1 in Hepatocytes**. (a)

839 Schematic illustrating the bi-transgenic, hepatocyte-specific, doxycycline (Dox)-inducible model

developed to express toxic CUG960i RNA in mouse livers. The $(CUG)_n$ repeat-containing transcripts sequester RNA-binding proteins, including MBNL proteins. Administration of Dox triggers the expression of toxic RNA in hepatocytes. This model is referred to as the DM1 liver model. (b) Experimental protocol for Dox diet feeding to induce DM1 in mouse livers, involving a 2g/kg Dox-supplemented diet until weaning on day 21, followed by a switch to a 0.1g/kg Dox diet or maintenance on the 2g/kg Dox diet for six weeks. Glucose tolerance testing (GTT) occurs a week before sacrifice. (c) Hybrid RNA fluorescent in-situ hybridization immuno-fluorescence (RNA FISH-IF) imaging depicts toxic $(CUG)_n$ RNA (red) and Mbnl1 (green) foci in hepatocyte nuclei (blue). (d) Quantification of CUG960i/Mbnl1 foci in hepatocyte nuclei via RNA FISH-IF. DM1 liver mice on 0.1g/kg Dox diet (n=7) are compared to the No Dox diet (n=5) and 2-week recovery mice (n=7). (e) Distribution of CUG960i/Mbnl1 foci per hepatocyte nucleus in mice fed 0.1g/kg Dox diet for one-month post-weaning (n=7). (f) Quantitative-PCR (qPCR) analysis of CUG960i RNA in hepatocytes and whole liver of DM1 liver mice and controls (ApoE-rtTA: n=5, DM1 liver mice: n=20, No-Dox mice: n=9, 2-week recovery mice: n=7). Box plots display first to third quartile with median line; mean ± SD for others. **P < 0.01.

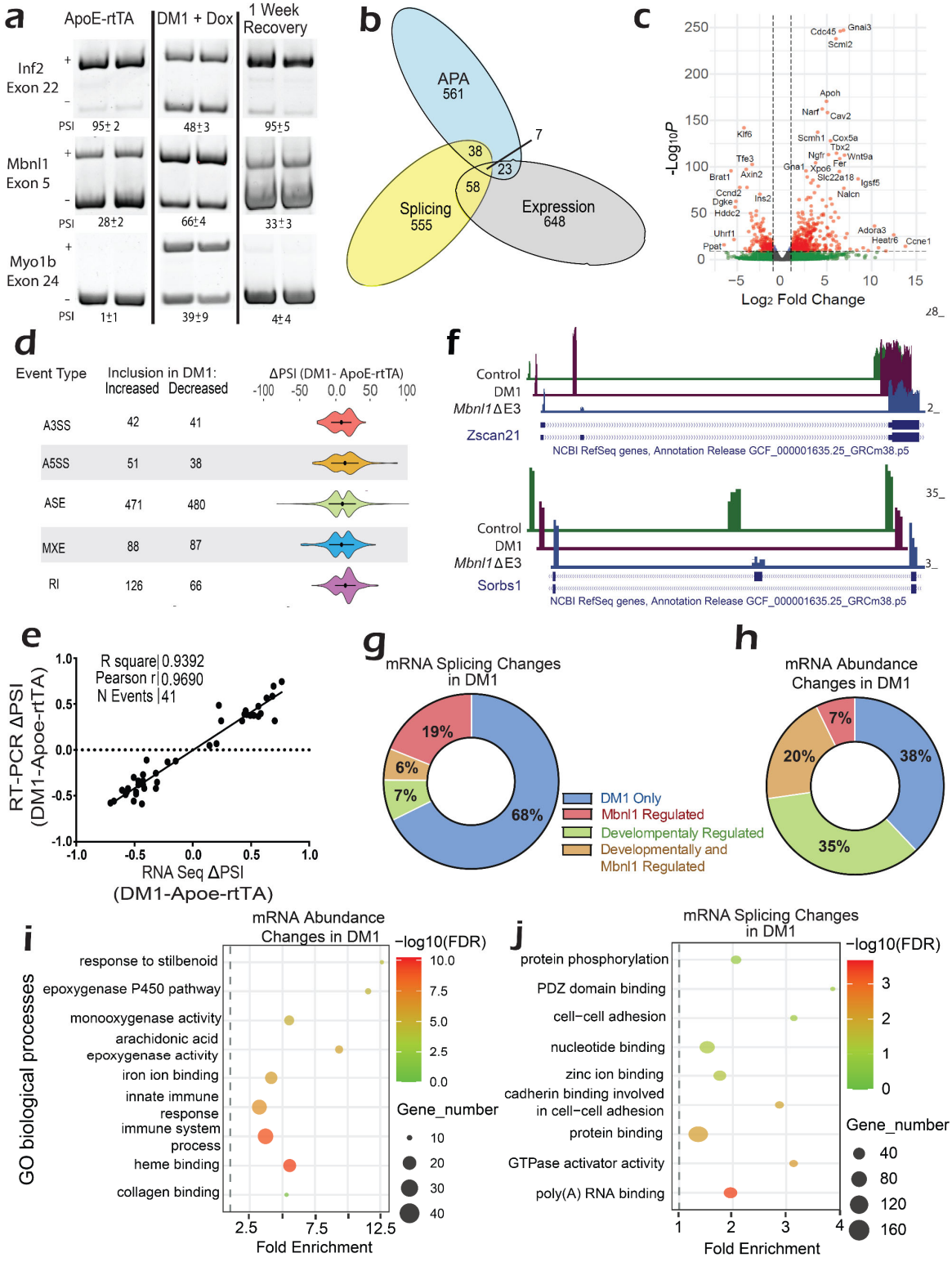

Fig. 2. DM1 Induces Global Transcriptomic Alterations in Hepatocytes. (a) RT-PCR splicing analysis of select MBNL1 targets. Bands indicate exon presence or absence, with (+)

for inclusion and (-) for exclusion. Targets are listed to the left of the image, with the percentage "spliced in" (PSI) below. (b) Overlap of alternative splicing, alternative polyadenylation (APA), and expression changes upon DM1 induction in hepatocytes. (c) Volcano Plot illustrating mRNA abundance changes from RNA-seq (d) Violin plots displaying inclusion levels of alternative splicing events from RNA-seq data. MXE = mutually exclusive, A3SS/ A5SS = alternative 3'/5', ASE = alternative cassette exon, and RI = retained intron. (e) Change in PSI determined by RT-PCR (y-axis) vs. RNA Seq analysis (x-axis) for 30 events. (f) Gene Tracks of representative genes showing alternative exon inclusion in DM1 liver, *Mbnl1*$^{\Delta E3/\Delta E3}$ (KO), or wild-type animals. (g) Pie chart – comparison of alternatively spliced genes regulated by DM1, Mbnl1, or maturation in the liver. (h) Pie chart – comparison of differentially expressed genes (DEG) regulated by DM1, Mbnl1, or maturation. (i) GO Diagram - mRNA Processing: Selected processes related to genes with alternative mRNA processing events in DM1 liver. (j) GO Diagram - Differential Expression: Processes related to genes undergoing differential expression in DM1 liver. n=3 for DM1 liver and controls, n=2 for MBNL1KO and controls.

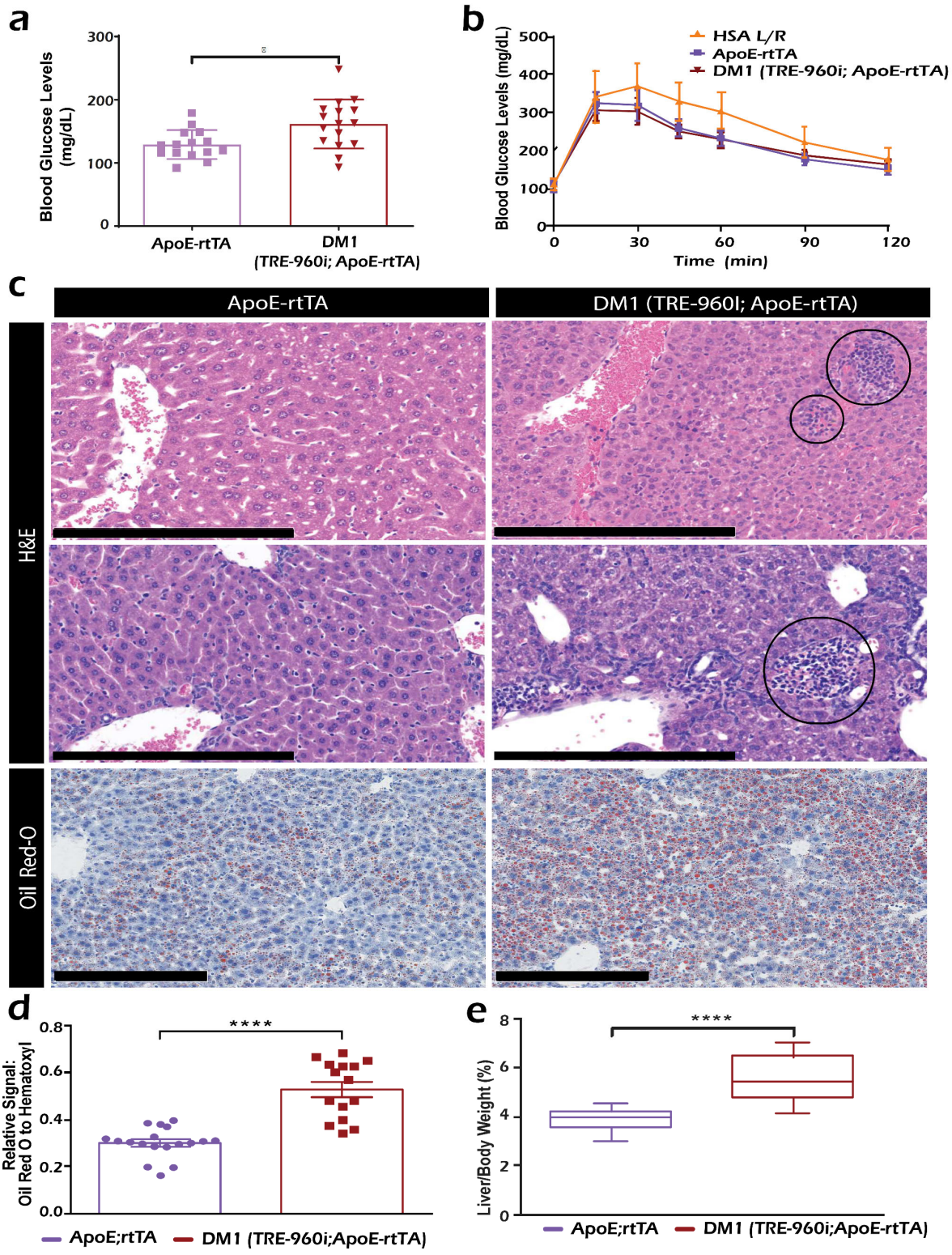

873

874 **Fig. 3. DM1 Induces Hepatic Lipid Accumulation and Injury.** (a) Blood glucose levels

875 measured before sacrifice after a 4-hour fast (n=15 for ApoE-rtTA mice and 16 for DM1 mice). (b)

Glucose tolerance testing (GTT) curves depicting blood glucose levels post-intraperitoneal glucose injection. GTT was performed a week before harvest following a 24-hour fast (n=14 for ApoE-rtTA mice, 13 for DM1 liver mice, and 18 for HSA L/R mice). (c) Representative histological images of ApoE-rtTA control and DM1 mice. Hematoxylin and eosin (H&E) images showcasing inflammation and necrosis in the DM1 liver, with inflammation and necrosis circled, are at the top. Oil Red-O images indicating lipid droplets (Red) with nuclei stained in hematoxylin (blue) are at the bottom. Black scale bars represent 200 μm. (d) Hepatosomatic index for DM1 mice and ApoE-rtTA controls (n=16 for ApoE-rtTA mice and 32 for DM1 liver mice). (e) Quantification of Oil Red O signal, relative to hematoxylin-stained nuclei, indicating lipid accumulation (n=18 for ApoE-rtTA mice and 15 for DM1 liver mice). Box plots show first to third quartile with median line; mean ± SD for all others. *P < 0.05, ****P < 0.0001.

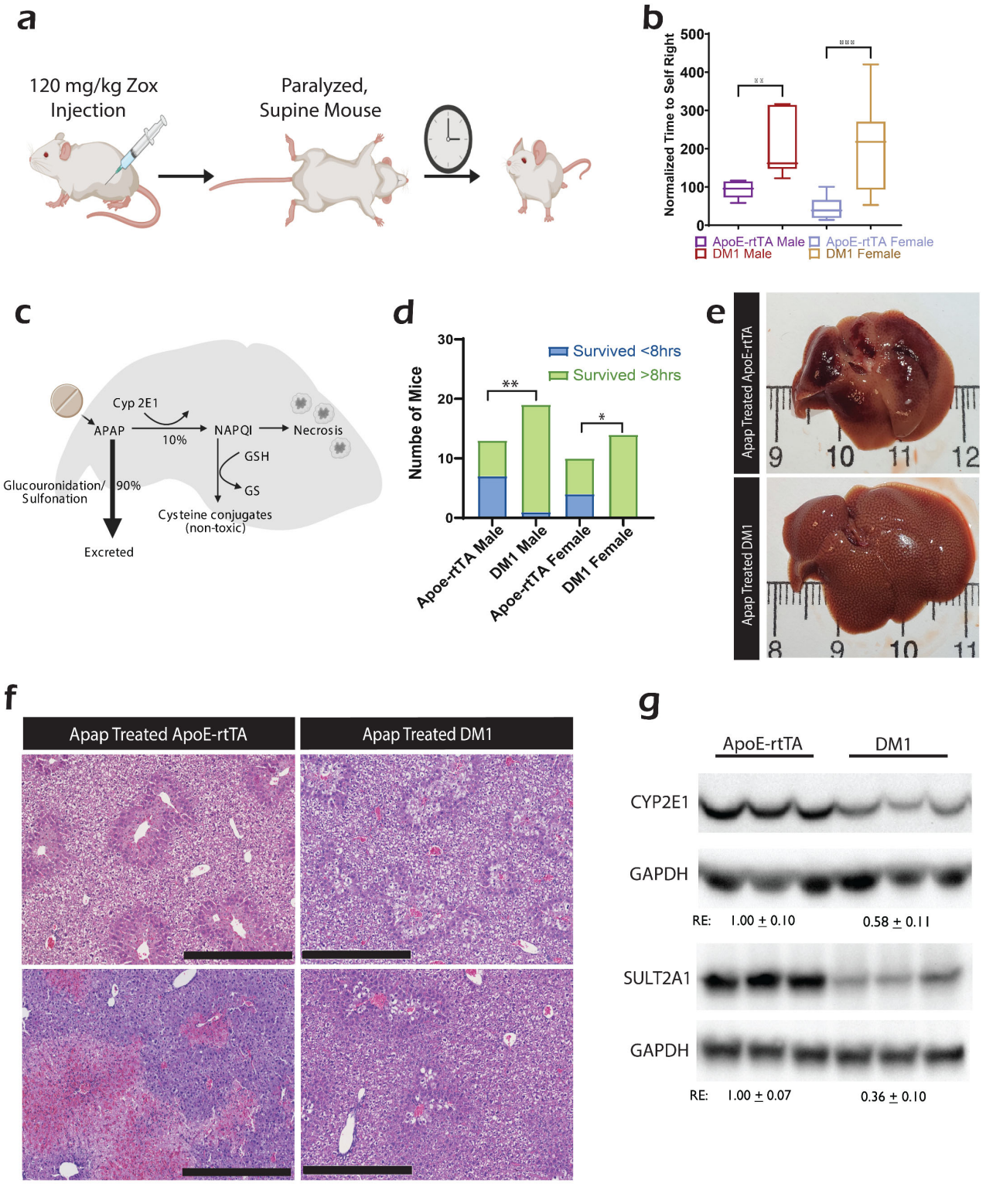

887

888 **Fig. 4. Impaired Drug Metabolism in DM1 Liver Model Mice.** (a) Schematic illustrating

889 zoxazolamine (Zox) testing procedure, measuring self-righting time post-IP injection of 120

mg/kg Zox. (b) Normalized average self-righting time of Zox-injected mice (n=9, 10, 7, 8 from left to right). (c) Diagram outlining APAP drug metabolism in hepatocytes. (d) Mortality rate 8 hours post 350 mg/kg APAP injection (n=13, 19, 10, 14 from left to right). (e) Representative livers of male mice surviving 24 hours post-APAP injection. (f) H&E images of livers from male mice 24 hours post-APAP injection. Black scale bars represent 200 μm. (g) Western blots showing CYP2E1 and SULT2A1 protein levels in control and DM1 mice. Box plots display first to third quartile with median line. *P < 0.05, **P < 0.01, ***P < 0.001.

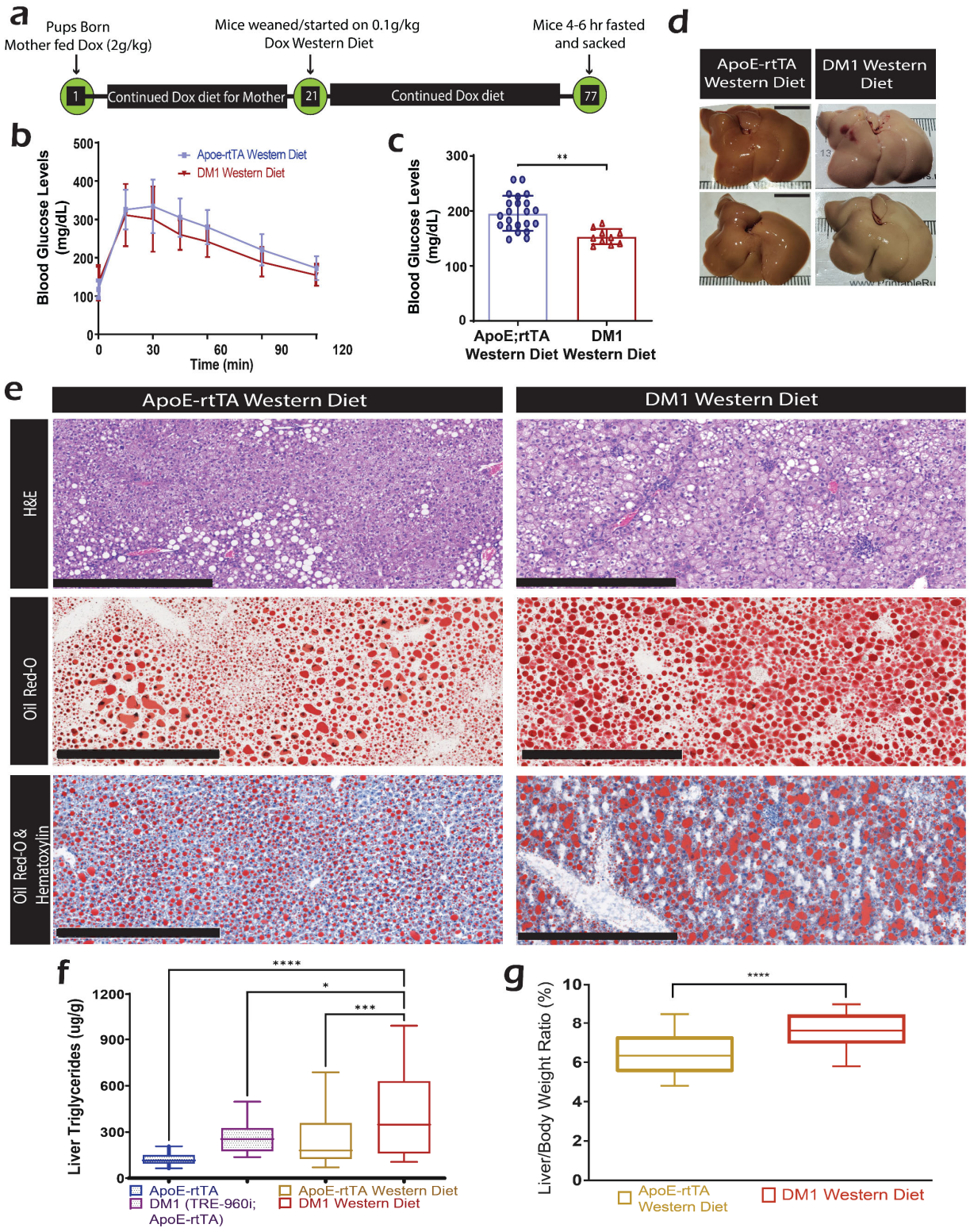

Fig. 5. DM1 Exacerbates Diet-Induced NAFLD Severity. (a) Schematic of the feeding protocol for mice on a Western diet, starting with a 2g/kg Dox-supplemented diet at birth and transitioning

to a 0.1g/kg Dox-supplemented high-fat, high-sugar "Western" diet at weaning, maintained for eight weeks until sacrifice. (b) GTT curves of male mice on the western diet, performed twice with a six-day interval (n=23 for ApoE-rtTA mice and 16 for DM1 mice). (c) Blood glucose levels before sacrifice after a 4-hour fast (n=22 for ApoE-rtTA mice and 10 for DM1 liver mice). (d) Representative liver images from ApoE-rtTA (left) and DM1 liver mice (right) on the Western diet. (e) Representative histological images, including H&E (Top) images with circled inflammation and necrosis in DM1 liver and Oil Red-O (Bottom two) images staining lipid droplets (Red) with nuclei in blue. Black scale bars represent 200 μm. (f) Analysis of extractable triglycerides in livers of mice on basal and western diets (n=21 for ApoE-rtTA mice and 14 for DM1 liver mice). (g) Hepatosomatic index for Western diet-fed DM1 mice and ApoE-rtTA mice (n=34 for ApoE-rtTA mice and 19 for DM1 liver mice). Values displayed as median to quartiles for box plots; mean ± SD for all others. *P < 0.05, **P < 0.01, ***P < 0.001.

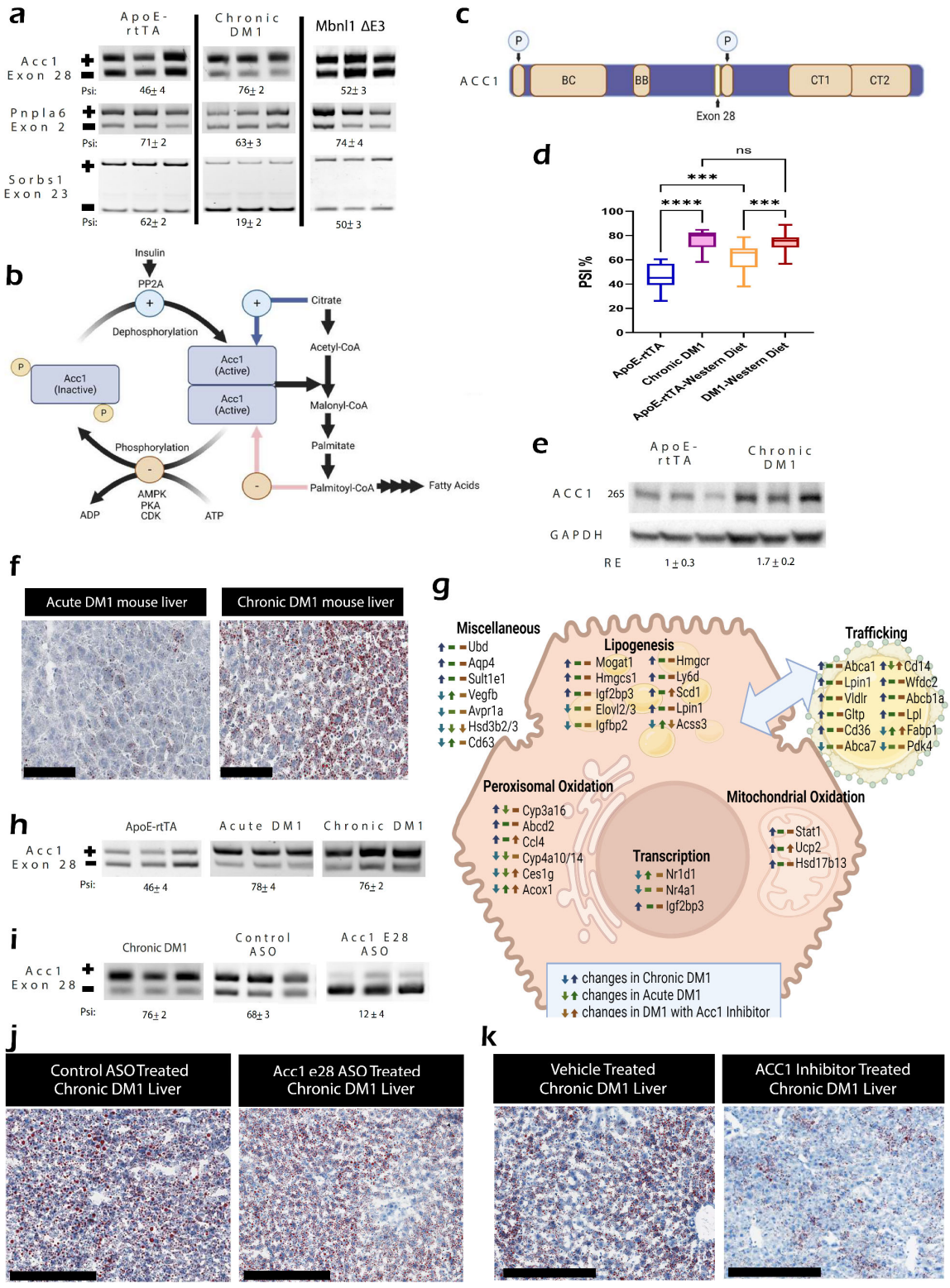

Fig. 6. DM1 Disrupts Liver Lipid Regulation and Drives Lipogenesis via Acetyl-CoA Carboxylase 1. (a) RT-PCR splicing gel analysis of select alternative splicing events in DM1-

afflicted livers. Target names are listed on the left, with PSI values below. (b) Diagram of acetyl-CoA carboxylase 1 (ACC1) regulation and function. ACC1, phosphorylated by kinases like AMPK and PKA, is inactivated. Upon insulin-driven PP2A dephosphorylation, ACC1 becomes active, converting acetyl-CoA into malonyl-CoA, which is further processed into palmitoyl-CoA and eventually fatty acids. (c) Schematic of selected genes with altered alternative splicing in DM1 livers, displaying locations of alternatively regulated exons and notable domains. Gene names are on the left. P = phosphorylation cluster; BC = biotin carboxylase domain; BB = biotin binding/biotin carboxylase carrier protein domain; CT = carboxyltransferase domain. (d) Percent inclusion of Acc1 exon 28 in chronic DM1 and controls and mice on a westernized diet (n=10, 13, 24, 21 from left to right). (e) Western blot showing Acc1 protein levels in chronic DM1 and control mice. (f) Lipid accumulation in acute and chronic DM1 mice livers via ORO staining. Black scale bars represent 50 μm. (g) Diagram summarizing gene abundance changes related to lipid regulation in livers of acute and chronic DM1 mice and chronic DM1 mice treated with Acc1 inhibitor CP-640816. Chronic DM1 mice transcripts compared to ApoE-rtTA mice fed 0.1g Dox for two months by RNA sequencing analysis. Acute DM1 and transcripts from DM1 mice treated with Acc1 inhibitor compared to chronic DM1 animals via qPCR. (h) RT-PCR splicing gel analysis of Acc1 exon 28 in acute and chronic DM1 mice livers. (i) Changes in Acc1 exon 28 inclusion in chronic DM1 mice treated with repeated doses of 12mg per kg body weight of either control antisense oligonucleotide (ASO) or Acc1 exon 28 targeting ASO. (j) ORO staining of chronic DM1 mice livers treated with Acc1 exon 28 or control ASO. Black scale bars represent 200 μm. (k) ORO staining from chronic DM1 mice treated with daily doses of 25μg of Acc1 inhibitor CP-640816 per kg of body weight or equivalent volume of vehicle. Black scale bars represent 200 μm. Values are displayed as median to quartiles for box plots. ***P < 0.001, ****P < 0.0001